Available online at www.sciencedirect.com
SCIENCE DIRECT
International Journal of Pharmaceutics 309 (2006) 157–162
INTERNATIONAL JOURNAL OF PHARMACEUTICS
www.elsevier.com/locate/ijpharm

# Pore size distributions of biodegradable polymer microparticles in aqueous environments measured by NMR cryoporometry

Oleg Petrov [a], István Furó [a], Michael Schuleit [b], Rainer Domanig [c], Mark Plunkett [d], John Daicic [d,*]

[a] *Division of Physical Chemistry and Industrial NMR Centre, Institute of Chemistry, School of Chemical Science and Engineering, Royal Institute of Technology, Teknikringen 30, SE-10044 Stockholm, Sweden*
[b] *Novartis Pharma AG, Pharmaceutical & Analytical Development, P.O. Box 4002, Basel, Switzerland*
[c] *Sandoz GMBH Biochemiestr. 10, 6336 Langkampfen, Austria*
[d] *YKI, Ytkemiska Institutet AB (Institute for Surface Chemistry), Box 5607, SE-114 86 Stockholm, Sweden*

Received 1 November 2005; received in revised form 16 November 2005; accepted 19 November 2005
Available online 28 December 2005

**Abstract**

NMR cryoporometry is a unique method permitting the investigation of pores in the microporous and mesoporous regimes for samples in aqueous environments. Here, we apply the technique to porous biodegradable polymer microparticles designed as devices for drug delivery in depot formulations. The results indicate that structural features too small to be captured in surface and fracture images obtained by SEM are able to be accessed using the technique, and that the evolution of pore structure can be studied for several days as the particles swell and degrade in the aqueous environment.


*Keywords:* Microparticles; Drug release; Pore size distribution; Swelling; Degradation; NMR cryoporometry; SEM

## 1. Introduction

Biodegradable polymers have been investigated extensively for their capability of releasing proteins and peptides in a controlled way over a period of several weeks or months. The most desirable release profile would show a constant release rate with time. The factors affecting the drug release rate include the structure of the matrix and the physicochemical properties of both the polymer and the drug. However, in many cases release profiles are more complicated and often contain two main features, the first being the initial drug burst and a second, usually more constant release rate, dependent on diffusion and degradation (Freiberg and Zhu, 2004). Drug release starts from the microparticle surface followed from the inner region of the material. Therefore, the drug burst is characterized by adsorbed drug on the particle surface or by a leaching out process of drug from larger pores close to the surface. The second release phase show a clear dependence on polymer molecular weight (Park, 1994) and crystallinity (Frank et al., 2004), drug load (Kakish et al., 2002), size distribution (Bezemer et al., 2000) and porosity (Yang et al., 2000). The porosity of a microparticle system will be determined during the preparation process and is known to affect the release kinetics. This was shown in a study where a highly porous matrix released drug at a higher rate than its less porous counterpart (Yang et al., 2000). Traditionally, scanning electron microscopy (SEM) and mercury porosimetry have been used to characterize microparticle porosities and morphologies. However, these methods have their specific disadvantages. SEM gives only information on pore sizes above a certain pore diameter, typically in the range of a few μm. Mercury porosimetry often provides incomplete information because mercury is a non-wetting liquid that is difficult to imbibe into small pores. The high pressure that has to be applied can deform the porous network and close small pores.

In recent years, additional analytical research tools have become available that make it possible to deal with the complexities of biodegradable microparticles. Structural features in the nanometer-to-micrometer size range can for example be

* Corresponding author. Tel.: +46 8 5010 6038; fax: +46 8 20 8998.
*E-mail address:* john.daicic@surfchem.kth.se (J. Daicic).

0378-5173/$ – see front matter © 2005 Elsevier B.V. All rights reserved.
doi:10.1016/j.ijpharm.2005.11.027

measured directly by NMR- or DSC-based cryoporometry (the latter sometimes is also called thermoporometry) (Ishikiriyama et al., 1995; Strange et al., 1993; Ishikiriyama and Todoki, 1995; Schreiber et al., 2001). This technology takes advantage of the size-dependent freezing/melting point depression encountered by materials encapsulated in small volumes within a matrix (Christenson, 2001; Jackson and McKenna, 1990). Of the two options (NMR and DSC), NMR, although more time-consuming, can be performed at any cooling/heating rate, and is probably the method of choice if the size range of the investigated structural features extends over 10 nm. In NMR cryoporometry, use is made of the fact the transverse relaxation time for the liquid NMR signal is several orders of magnitude longer than that for solid. By determining the amount of liquid at different temperatures, an apparent pore size distribution can be calculated. By choosing water as probe liquid, another advantage of this novel technology becomes the possibility to determine pore size distributions in the presence of water, which offers the opportunity to monitor the change in size distribution as a function of time and to therefore mimic in vivo conditions. The ease of application of the technique to in situ studies of degradation is a clear advantage over techniques such as gas adsorption and mercury porosimetry, where intermediate steps involving sample drying and conditioning would need to be undertaken. It should be noted that a detailed comparative study of the DSC cryoporometry technique with these other methods has been performed on model porous glass systems (Ishikiriyama and Todoki, 1995), and that the NMR and DSC cryoporometry methods have recently been compared to mercury porosimetry measurements on compacts formed from ground calcium carbonate (Gane et al., 2004). The technique has been applied to inhomogeneous porous products in other technical areas, e.g. paper (Furó and Daicic, 1999). A related method is NMR diffusometry, which has been used to study non-freezing water in biological porous materials (Topgaard and Söderman, 2002).

The NMR cryoporometry technique can be considered as one of several new applications of NMR physical characterization methods to pharmaceuticals; recent developments in this area have mainly focused on magnetic resonance imaging (MRI) for in vitro and in vivo studies (Richardson et al., 2005). NMR cryoporometry provides a complementary, quantitative analysis of pore size in the nanometer range (micropores and mesopores), a regime where imaging techniques have yet to achieve sufficient resolution to access. The importance of micropores and mesopores has not been considered in the past due to the fact that no measuring methods have been available. However, small pores in the nanometer size range increase significantly the internal surface-to-volume ratio, which affects polymer hydration and consequently degradation of the originally water-insoluble polymer into water-soluble fragments.

An increased degree of hydration influences directly the attractive interactions between the polymer and drug, as the hydrophobic matrix polymer develops hydrophilic interaction sites. This in turn can influence drug release kinetics, since increased attractive interactions between the polymer and drug prevent fast drug diffusion from the material (Boury et al., 1997). Therefore, it is of great importance to gain a better understanding of the in situ evolution of porosity on different length scales during polymer degradation, which may permit a more precise prediction of drug release from microparticles. Furthermore, in a broader perspective, the possibility to accurately characterize meso- and micropores becomes of increasing importance as developments in nanotechnology accelerate and provide new formulation strategies. For example, biodegradable particles around 100 nm in size have been prepared, which demonstrate relatively faster polymer degradation during the initial phase compared to larger microparticles (Panyam et al., 2003).

With respect to the importance of porosity for the development of both micro- and nanosized biodegradable depot formulations, the aim of our work was to develop and apply a method that allows an assessment of the internal porosity in the nanometer size range. For this reason, structurally defined poly(D,L-lactide-co-glycolide) microparticles have been produced which showed relatively dense internal morphologies when investigated with scanning electron microscopy (SEM), indicating a low degree of porosity in the range accessible to that method, i.e. larger than several μm.

## 2. Materials and methods

### 2.1. Sample preparation

A series of porous polymeric particles manufactured by an organic phase separation process (coacervation) have been investigated (see Table 1). An amount of 4.1 g poly(D,L-lactide-co-glycolide) star polymer (Novartis, Basel) was dissolved in dichloromethane (Aldrich, 99.6%, ACS) in a 750 mL glass reactor provided with a glass stirrer. An appropriate amount of drug substance (DS, Novartis, Basel) was dissolved in methanol (Fluka, Puriss p.A.) and introduced with stirring to the solution of polymer, followed by addition of silicon fluid (Wacker, Pharsil) as a phase-separation inducer. The soft embryonic microspheres, produced by this procedure, were hardened by transferring into a heptane/water emulsion with ongoing stirring. The microspheres were collected on a G3 sintered glass filter. Prior to the main drying step (<50 °C) mannitol (Mallinckrodt, powder 6208) was added to the product to reduce agglomeration. It should be noted that the only differences with respect to sample preparation are those listed in Table 1, i.e. for samples A–E containing DS, the variation is limited to polymer molecular weight (average and polydispersity), and that samples F and G

Table 1
Samples investigated in the study

| Sample | Composition | Polymer MW | Polydispersity |
|---|---|---|---|
| A | Polymer, DS, mannitol | 50800 | 1.71 |
| B | | 61900 | 1.64 |
| C | | 59900 | 1.77 |
| D | | 51300 | 1.8 |
| E | | 55800 | 1.78 |
| F | Polymer, mannitol | 56100 | 1.73 |
| G | | 59500 | 1.79 |

Table 2
NMR sample characteristics

| Sample | Composition (mg) | | Swelling time (days) | Water bound in gel (%) | Degree of swelling[a] |
|---|---|---|---|---|---|
| | Dry polymer | Water | | | |
| A1 | 29.8 | 51.0 | 1 | 43 | 0.74 |
| A2 | 29.6 | 53.3 | 3 | 47 | 0.85 |
| A3 | 31.2 | 52.4 | 4 | 53 | 0.89 |
| B1 | 31.0 | 52.3 | 1 | 47 | 0.79 |
| B2 | 30.6 | 51.6 | 3 | – | – |
| B3 | 29.8 | 52.5 | 4 | 72 | 1.27 |
| C1 | 30.6 | 54.1 | 1 | 57 | 1.01 |
| C2 | 31.5 | 57.2 | 3 | 48 | 0.87 |
| C3 | 32.0 | 53.6 | 4 | 45 | 0.75 |
| D1 | 30.4 | 59.2 | 1 | 23 | 0.45 |
| D2 | 30.4 | 59.5 | 3 | 25 | 0.49 |
| D3 | 31.9 | 58.7 | 4 | 28 | 0.52 |
| E1 | 31.4 | 53.9 | 1 | 35 | 0.60 |
| E2 | 32.0 | 52.7 | 3 | 36 | 0.59 |
| E3 | 32.4 | 53.4 | 4 | 39 | 0.64 |
| F1 | 30.1 | 53.8 | 1 | 38 | 0.68 |
| F2 | 31.0 | 54.2 | 3 | <6 | <0.1 |
| F3 | 28.7 | 54.4 | 4 | [b] | [b] |
| G1 | 32.0 | 51.6 | 1 | [b] | [b] |
| G2 | 31.9 | 55.0 | 3 | [b] | [b] |
| G3 | 31.3 | 51.8 | 4 | [b] | [b] |

[a] Water in gel in mg for 1 mg of dry polymer.
[b] Polymer dissolution instead of swelling.

were produced following the same procedure, but contain no DS (placebos).

For the cryo-NMR measurements, a small amount of dry polymer powder was placed at the bottom of a 10 mm NMR tube, Millipore water added without mixing, and the sample was left to swell at room temperature. Three samples, to be measured after swelling for 1, 3 and 4 days, were prepared separately for each polymer. The reason for this (instead of using the same sample) is that repeated freezing–thawing often changes the structure of porous materials (Allen et al., 1998). The sample characteristics are given in Table 2. With those compositions, the samples contained a swollen polymer region at the bottom of the tube and a supernatant primarily of water. A fraction of water confined in the gel phase (Table 2) was estimated from the NMR cryoporometry measurements based on its melting point depression, as illustrated in Fig. 1. A small amount of non-freezing water was also observed (~1% at 230 K), which was attributed to water molecules strongly bound to the polymer (Guan et al., 1996).

### 2.2. NMR measurements

The NMR cryoporometry experiments were carried out on a Bruker DMX200 NMR spectrometer equipped with a BVT-3000 temperature controller. The temperature of the samples in the NMR probe was controlled by a precision of ±0.1 K. The temperature spread over the samples of <5 mm height was estimated from the bulk water transition width to ≤0.1 K. During an experiment, the integral intensity of the NMR signal of the liquid phase was measured at different temperatures. The liquid water signal was extracted by $T_2$-filter implemented in a spin–echo experiment with pulse sequence $T$–$90_x$–$\tau$–$180_y$–$\tau$–echo, and $T = 2$ s and $\tau = 10$ ms. The samples were first cooled during 40–50 min down to 230 K and thereafter the integral intensity of the liquid water NMR signal, $I(T)$, was recorded upon increasing the temperature at a rate of 0.1 K/5 min (outside phase transition regions) and 0.1 K/45 min (in phase transition regions).

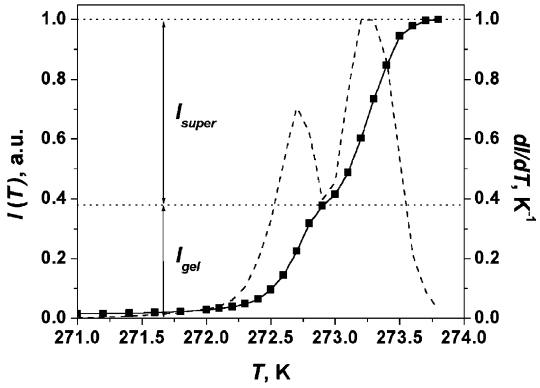


Fig. 1. The percentage of non-frozen water as a function of temperature (solid squares) and its derivative (dashed line) obtained in NMR cryoporometry experiment on sample F1.

The pore size distribution, $p(d)$, in the gel phase was calculated from $I(T)$ using the Gibbs–Thompson relation for the melting point depression as (Strange et al., 1993):

$$p(d) = \frac{K}{d^2}\frac{\partial I}{\partial T} \quad (1)$$

where $d$ is an effective diameter for assumedly cylindrical pores, and the material constant $K$ ($=2\nu\gamma_{sl}T^0/\Delta H$), where $\nu$ is the molar volume, $\gamma_{sl}$ the free energy of the solid–liquid interface, and $\Delta H$ is the latent heat of melting of the pore-filling material of water set to the generally accepted value of 50 K nm. The melting point of the excess bulk water $T^0$ served as the reference temperature.

### 2.3. Scanning electron microscopy (SEM)

The morphology of the samples were examined and photographed using a scanning electron microscope (JEOL JSM 6300). The samples were placed on a sample holder and sputter-coated with gold/palladium.

### 2.4. Size exclusion chromatography (SEC)

Average molecular weight and polydispersities of the polymer were determined by size exclusion chromatography (SEC). The data collection and analysis were done using Waters Millennium 32 software. Peak slicing was used to calculate the weight average ($M_w$) and the number average molecular weights ($M_n$). THF, with a flow rate of 0.8 mL/min, was used at 35 °C as an eluent. Polystyrene standards have been used for calibration.

### 2.5. Dissolution studies

A precisely weighed amount of microspheres was suspended in 5 mL of an acetic acid buffer solution adjusted to pH 4 in a 12 mL culture tube, equipped with a screw cap with a Teflon-coated septum. This tube is attached to a Van der Kamp sustained release apparatus and rotated at fixed velocity and temperature. After defined intervals, e.g. 24 h, the drug content of an aliquot of the solution is analyzed by HPLC. As the total drug content of the microspheres is known (measured in extra analyses) the dissolution rate may then be calculated.

## 3. Results

Fig. 1 represents a typical *I–T* curve obtained in NMR cryoporometry experiments. Two steps occur in this curve leading to two separate peaks in its derivative: one centered about 272.7 K and one at 273.2 K. We assign the steps to those for the melting

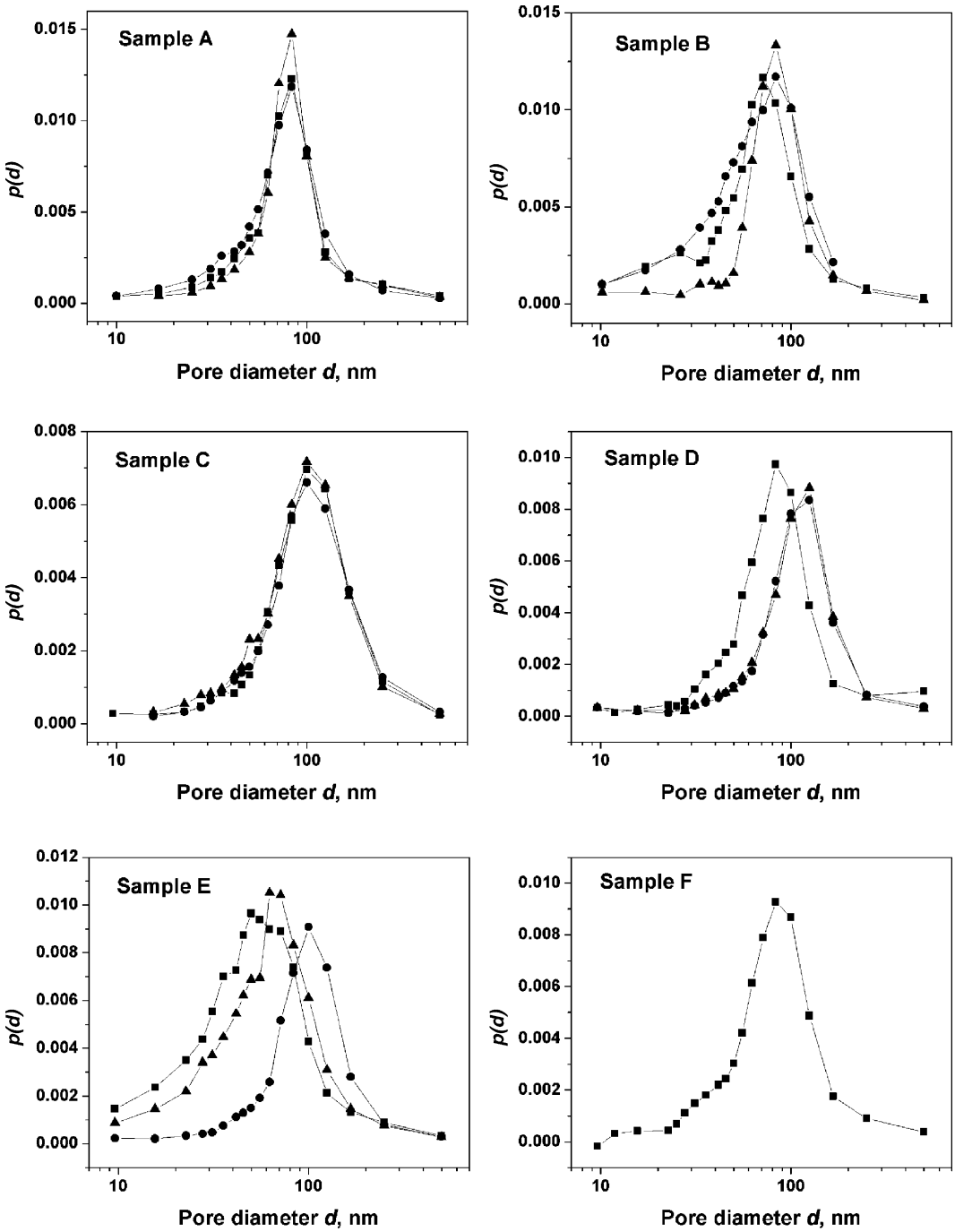


Fig. 2. The pore size distributions in the polymer/gel phases for samples A–F, after swelling for 1 day (squares), 3 days (circles) and 4 days (triangles). The areas were normalized to unity. Note the logarithmic scale. For sample F, the distribution is only given after 1 day since at longer times the sample peak and the supernatant bulk peak blend into one. For the same reason sample G was not shown at all (i.e. only a single peak after swelling for 1 day).

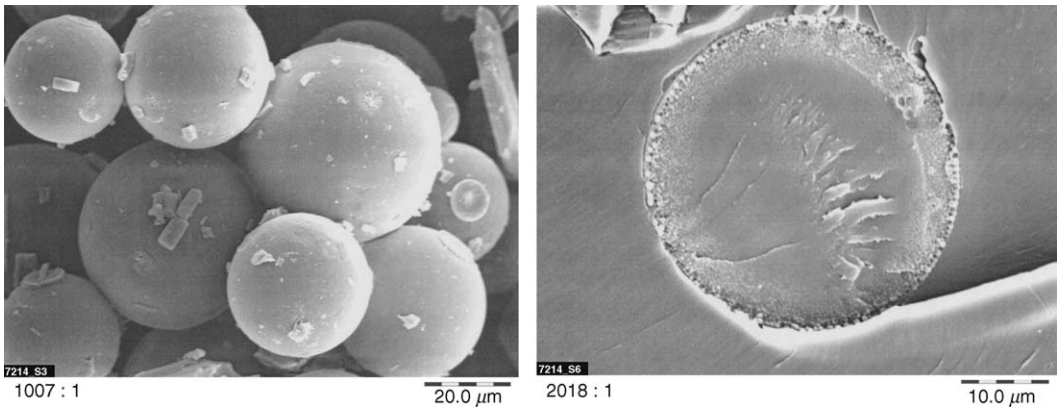


Fig. 3. Surface (left) and internal (right) structure of sample A studied by SEM. The fracture image to the right reveals some subsurface pores, but pores deeper in the interior are not visible. The 24 h drug release was 0.8%.

of water bound in the swollen polymer/gel phase and for the melting of the bulk supernatant water, respectively. As such it was possible to calculate the relative amount of water bound in gel (denoted as $I_{gel}$ in Fig. 1) and thereby the degree of swelling for both different samples and different ages of the samples, as shown in Table 2. On the other hand, the occurrence of two distinct steps in the *I–T* curve as an attribute of the presence of a polymer gel network enables us to monitor the process of its degradation.

The results are first presented as the evolution of the polymer network after swelling for 1, 3 and 4 days, for each sample. The placebo sample F showed a swelling behavior that differed from those of the active samples; we suggest that it swells more than the other materials and approaches a homogeneous polymer solution state after a long period of swelling. After 4 days, we could not identify at all, in contrast to case for the other samples, two clear and distinct melting steps (see Fig. 1) for the water in the sample. Similarly, the other placebo sample G did not show two clear and distinct melting steps that could correspond to water in gel and in supernatant. Note that this could also mean, in the eventuality that the porous gel matrix indeed remained, pore sizes out of the range of NMR cryoporometry (>500–600 nm).

Fig. 2 shows the evolution of the pore size distribution during swelling, for the different samples. It is important to note that traditionally the technique is used to investigate pores up to 100 nm diameter and yet in these experiments the pores are determined up to ≈600 nm. Since the uncertainty in the pore diameters becomes larger with larger pores (due to the relationship between the melting point suppression and the pore diameter) it is acknowledged that the actual pore diameters above 100 nm are only approximate. However, it can be stated there is an actual detectable peak in the pore diameters (around 100 nm) and hence, due to the data quality, the pore distributions are shown up to 600 nm to illustrate this.

In order to compare the pore size evolution to the morphology of the samples, we present SEM images of a selection of the samples investigated. We choose sample A (Fig. 3) and sample E (Fig. 4) that showed a respectively static and changing pore size evolution over 4 days.

## 4. Discussion

It is worthwhile noting that the images presented in Figs. 3 and 4 give little indication of a pore structure where up to over 50% of the sample can be filled with water after 1 day of absorption (see Table 2). The fracture image for sample A indicates some surface porosity, but deeper internal pores of the order of ≈100 μm in size are not visible. Overall, the NMR measurements indicate a pore structure that is conducive to the

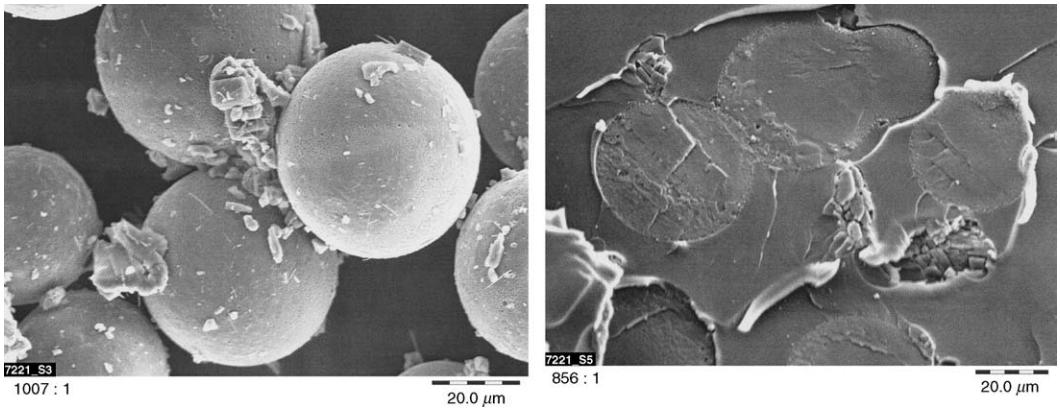


Fig. 4. Surface (left) and internal (right) structure of sample E studied by SEM. The 24 h drug release was in this case 2.9%.

imbibition of water and permits a significant pore swelling over the period of several days.

The 24 h drug release amounted 0.8% for sample A and 2.9% for sample E. The difference in the drug release might not be attributed to the presence of nanosized pores only. Adsorbed drug on the microparticle surface might contribute also to drug release in the initial phase. However, comparing the pore size distribution of both samples (Fig. 2A and E), the sample E shows significantly higher intensities in the nanometer size range between 30 and 70 nm after 24 h compared to sample A. This observation tempts us to speculate that the increased number of nanosized pores indicates the presence of a pore network, which might favor a rapid swelling and thereby promote a faster drug release. Moreover, the large interfacial area that is a consequence of a significant volume of nanosized pores would tend to favor higher release rates also due to the fact that this would increase the relative amount of the most mobile drug substance molecules, which reside at the solid–liquid interface.

Although some differences were observed for the evolution of the pore size distribution of micro- and mesopores for samples A–E, a connection to underlying causes for these differences would be at best speculative. As noted, the only variation in the preparation of these samples was the molecular weight of the polymer, and it is difficult to see any correlation to the molecular weight distribution data in Table 1. The samples may however be classed in two groups: samples A–C show a relatively static pore size distribution, whereas samples D and E evolve over the timescale of several days. On the other hand, the placebo samples F and G showed a very different tendency to rapidly swell and disintegrate, indicating that inclusion of the DS changes the polymer–polymer interaction in the microparticle matrix.

The aim of this paper is to introduce NMR cryoporometry as a novel sensitive analytical method which allows a reproducible evaluation of pores in nanometer size range in polymeric depot formulations. The described technique provides a means by which to access, in an aqueous environment, a pore size range that is inaccessible to other methods. Moreover, the total volume of pores in this regime was seen to be significant, with implications for the drug release. Based on the promising results in this work the next steps, now under way, include further studies of dense microparticles on longer time scales with the aim to investigate the relationship between nanosized pores and drug release in more detail.

## Acknowledgements

The authors wish to thank K. Paulus and Y. Duchesne for performing the scanning electron microscopy studies and the molecular weight measurements, respectively.

## References

Allen, S.G., Stephenson, P.C.L., Strange, J.H., 1998. J. Chem. Phys. 108, 8195–8198.
Bezemer, J.M., Radersma, R., Grijpma, D.W., Dijkstra, P.J., van Blitterswijk, C.A., Feijen, J., 2000. J. Contr. Release 67, 249–260.
Boury, F., Marchais, H., Proust, J.E., Benoit, J.P., 1997. J. Contr. Release 45.
Christenson, H.K., 2001. J. Phys. Conden. Matter 13, R95–R133.
Frank, A., Rath, S.K., Boey, F., Venkatran, S., 2004. Biomaterials 25, 813–821.
Freiberg, S., Zhu, X.X., 2004. Int. J. Pharm. 282, 1–18.
Furó, I., Daicic, J., 1999. Nordic Pulp. Paper Res. J. 14, 221–225.
Gane, P.A.C., Ridgeway, C.J., Lehtinen, E., Valiullin, R., Furó, I., Schoelkopf, J., Paulapuro, H., Daicic, J., 2004. Ind. Eng. Chem. Res. 43, 7920–7927.
Guan, Y.L., Shao, L., Yao, K.D., 1996. J. Appl. Polym. Sci. 61, 393–400.
Ishikiriyama, K., Todoki, M., 1995. J. Colloid Interface Sci. 174, 103–111.
Ishikiriyama, K., Todoki, M., Kobayashi, T., Tanzawa, H., 1995. J. Colloid Interface Sci. 173, 419–428.
Jackson, C.L., McKenna, G.B., 1990. J. Chem. Phys. 93, 9002–9011.
Kakish, H.F., Tashtoush, B., Ibrahim, H.G., Najib, N.M., 2002. Eur. J. Pharm. Biopharm. 54, 75–81.
Panyam, J., Dalii, M.M., Sahoo, S.K., Ma, W., Chakravarthi, S.S., Amidon, G.L., Levy, R., Labhasetwar, J.V., 2003. J. Contr. Release 92, 173–187.
Park, T.G., 1994. J. Contr. Release 28, 121–129.
Richardson, J.C., Bowtell, R.W., Mäder, K., Melia, C.D., 2005. Adv. Drug Delivery Rev. 57, 1191–1209.
Schreiber, A., Ketelsen, I., Findenegg, G.H., 2001. Phys. Chem. Chem. Phys. 3, 1185–1195.
Strange, J.H., Rahman, M., Smith, E.G., 1993. Phys. Rev. Lett. 71, 3589–3591.
Topgaard, D., Söderman, O., 2002. Biophys. J. 83, 3596–3606.
Yang, Y., Chung, T.S., Bai, X.-L., Chan, W.-K., 2000. Chem. Eng. Sci. 55, 2223–2236.